


3D PRINTING OF BIOMEDICAL MATERIALS AND DEVICES



3D printed poly(hydroxybutyrate-co-hydroxyvalerate)—45S5 bioactive glass composite resorbable scaffolds suitable for bone regeneration

Beatriz Aráoz^{1,6,a)} , Emine Karakaya³, Ana González Wusener⁵, Rainer Detsch³, Juan Bizzotto^{2,4}, Geraldine Gueron^{2,4}, Aldo R. Boccaccini^{3,a)}, Élica B. Hermida^{1,6}

¹Laboratory of Biomaterials, Biomechanics and Bioinstrumentation (Lab3Bio), School of Science & Technology (ECyT), National University of San Martín (UNSAM), 25 de Mayo 1143 (1650), Campus Miguelete, San Martín, Buenos Aires, Argentina

²Universidad de Buenos Aires, Facultad de Ciencias Exactas y Naturales, Departamento de Química Biológica, Intendente Guiraldes 2160, C1428EGA, Buenos Aires, Argentina

³Institute of Biomaterials, Department of Materials Science and Engineering, Friedrich-Alexander-University Erlangen-Nuremberg, Cauerstr. 6, 91058 Erlangen, Germany

⁴CONICET - Universidad de Buenos Aires, Instituto de Química Biológica de la Facultad de Ciencias Exactas y Naturales (IQUIBICEN), Ciudad Universitaria, Pabellón 2, 4to. Piso, Intendente Güiraldes 2160, C1428EGA Buenos Aires, Argentina

⁵Instituto de Investigaciones Biotecnológicas (IIBIO), Universidad Nacional de San Martín and Consejo Nacional de Investigaciones Científicas y Técnicas (CONICET), 25 de Mayo 1143 (1650), Campus Miguelete, San Martín, Buenos Aires, Argentina

⁶Instituto de Tecnologías Emergentes y Ciencias Aplicadas (ITECA), UNSAM, CONICET, ECyT, San Martín, Buenos Aires, Argentina

^{a)}Address all correspondence to these authors. e-mails: baraoz@unsam.edu.ar; aldo.boccaccini@ww.uni-erlangen.de

Received: 17 April 2021; accepted: 9 June 2021

Aldo R. Boccaccini was an editor of this journal during the review and decision stage. For the JMR policy on review and publication of manuscripts authored by editors, please refer to <http://www.mrs.org/editor-manuscripts/>.

3D printing for tissue engineering requires biomaterials with mechanical and biological properties suitable for both tissue regeneration and the printing process. A filament made of poly(hydroxybutyrate-co-hydroxyvalerate) (PHBV) combined with 45S5 Bioglass (BG) was used to print 3D scaffolds by fused deposition modeling (FDM). Chemical treatment of BG particles with chlorotrimethylsilane (CTMS) improved the ductility of the extruded filaments and allowed excellent printability. Controlling the printing parameter infill density ($I_{\%}$), from 20 to 90%, scaffolds were obtained with interconnected pores and channel sizes in the 100–800 μm range and exhibiting tensile modulus from 0.25 to 1.36 GPa. PHBV + BG scaffolds and PHBV scaffolds coated with CTMS treated BG particles, as a model of a rough and biologically active coating, showed no cytotoxic effects, and cells preferred the scaffolds containing BG in terms of cell spreading. Mechanical and biological properties of the scaffolds were similar to those of the extracellular matrix (ECM) of trabecular bone.

Introduction

3D printing is a powerful technique increasingly applied to solve clinical needs. The multiple applications of 3D printing are based on patient-specific solutions, mainly: presurgical personalized models, surgical guides, customized implants, and prosthetic limbs. It also contributes to expanding knowledge in tissue engineering, in medical education and in the testing of pharmaceutical or cosmetic products [1]. Since 3D printing plays an important role in the generation of scaffolds to replace damaged

bone, selection of biomaterials with mechanical and biological properties suitable for bone regeneration and 3D printing is essential. Scaffolds that mimic the extracellular matrix (ECM) of the desired tissue and that exhibit degradation kinetics compatible with tissue growth are required. In the case of bone, the ECM is mainly composed of hydroxyapatite (HA), a crystalline inorganic material that provides rigidity to bone, and collagen, a natural polymer that gives elasticity and toughness to the composite. The bone structure exhibits a hierarchical distribution of interconnected pores that allow: (i) the anchoring

and proliferation of bone cells, (ii) the exchange of nutrients and waste, and (iii) vascularization. Bone elastic modulus varies between ca. 0.05 GPa and ca. 20 GPa, depending on whether it is trabecular or cortical bone, as well as on the age and health status of the patient, among other factors [2].

A promising type of biomaterials for bone regeneration arises from the combination of a bioactive amorphous ceramic, e.g. bioactive glass (BG), and a biodegradable and biocompatible biopolymer from the polyhydroxyalkanoates family, e.g. poly(hydroxybutyrate-co-hydroxyvalerate) (PHBV) [3, 4]. Regarding BG, Hench et al. developed the 45S5 BG (45SiO₂-24.5Na₂O-24.5CaO-6P₂O₅ (wt%)) composition in 1971. In contact with biological fluids, 45S5 BG experiences surface reactions that lead to the formation of an HA layer similar to that existing in bone [5, 6]. The HA layer allows the biomaterial to be bond to bone tissue in a process called osteoconduction. Moreover, several studies have demonstrated that BG is also an osteoinducer [7], that is, BG leads to the up-regulation and activation of families of genes in osteoprogenitor cells that give rise to rapid bone regeneration, controlling the cell cycle of osteoblasts towards osteogenic differentiation and increasing osteoblast proliferation. These features shift the paradigm in the treatment of bone damage (see for example [8]). Despite its excellent chemical and biological properties, BG is extremely fragile to resemble the ECM of bone. Thus, a composite that combines BG with a tough polymeric matrix has been proposed as a proper material for mimicking the ECM of bone [9]; PHBV is a biopolymer with suitable properties to become the matrix of composite scaffolds for bone tissue engineering. In fact, this polymer, produced by bacterial fermentation, is piezoelectric [10], non-cytotoxic, and can be biodegraded by the body into metabolites. The degradation rate can be controlled by the valerate content and the morphology of the scaffold. Typically, a degradation time of around 2 years is sufficient for the formation of new bone [11, 12].

Regarding the scaffold fabrication, salt leaching, solvent evaporation, electrospinning, lyophilization have been used to build scaffolds that mimic the bone structure. More recently, 3D printing has become the technique of choice to manufacture custom-made scaffolds from images by Magnetic Resonance Imaging (MRI) or Computed Tomography (CT) of the bone to be replaced or repaired [13]. Fused deposition modeling (FDM) is a popular 3D printing technique used to get complex structures and is based on the layer-by-layer deposition of the desired material. This is, on one hand, because 3D printers are normally affordable devices and, on the other hand, due to a great deal of experience about the use of FDM for countless applications. Regarding the FDM printing procedure, a thermoplastic material is provided in the form of a filament and fused through a nozzle with a hot end. Composite filaments made by extrusion reduce cytotoxicity, manufacturing costs, and

negative environmental effects since neither chlorinated solvents nor surfactants are used. Furthermore, proper interfacial adhesion between polymer and filler can be achieved by the surface modification of the filler particles, improving the mechanical properties of the filaments. The printed structure can be partially or completely filled simply by varying the infill density ($I_{\%}$); this parameter, measured in percentage, defines the air gap between rasters of each printed layer. The $I_{\%}$ is a key parameter for the application of FDM in tissue engineering as it leads to structures with well-defined size and distribution of pores. Although recent work focused on poly(hydroxyalkanoates) as a suitable material for 3D printing by FDM [14–16], to the authors' knowledge, 3D printable filaments of PHBV + BG have not been reported in the literature yet.

Thus, this work aims to build and characterize the mechanical properties of 3D printed scaffolds made of PHBV and 45S5 BG that mimic the morphology and mechanical properties of the ECM of trabecular bone. In addition, pretreatment of the BG particles with a silylating agent is proposed to enhance the flexibility of the composite filaments as well as the surface roughness. Finally, the effect of BG on the viability of cells typically used in the context of bone regeneration biomaterials is discussed.

Results

BG treatment

To study the treatment of the BG particles with CTMS, the treated and untreated BG powders were analyzed by FTIR and WAXS. Figure 1a top panel shows the ATR-FTIR spectra of the CTMS-treated BG. The spectra were analyzed to identify functional groups. A broad band composed of two double peaks in the spectral range of 1100–900 cm⁻¹ and another band at 480 cm⁻¹, both attributed to the vibrations of Si–O–Si and phosphate groups present in amorphous BG were observed [17–20]. This spectrum did not show the characteristic bands of C–H stretching that would be expected as markers of the success of the silylation process as a signal at 2850–3000 cm⁻¹. For this reason, the diffuse reflectance of IR beams by the powder was measured using the DRIFT accessory, which is a spectroscopic technique more sensitive to the chemical composition of the particle surface. The inner panel shows DRIFT spectra of untreated BG (red line) and treated BG (black line). The DRIFT spectra of treated and untreated BG are similar around 2850–3000 cm⁻¹, thus, the DRIFT spectra do not show a clear silylation reaction on the surface of the BG particles. As shown in Fig. 1b, peaks in the diffractogram remark the crystallinity differences between the treated (black line) and untreated BG (red line). In the latter, only the amorphous halo appears while

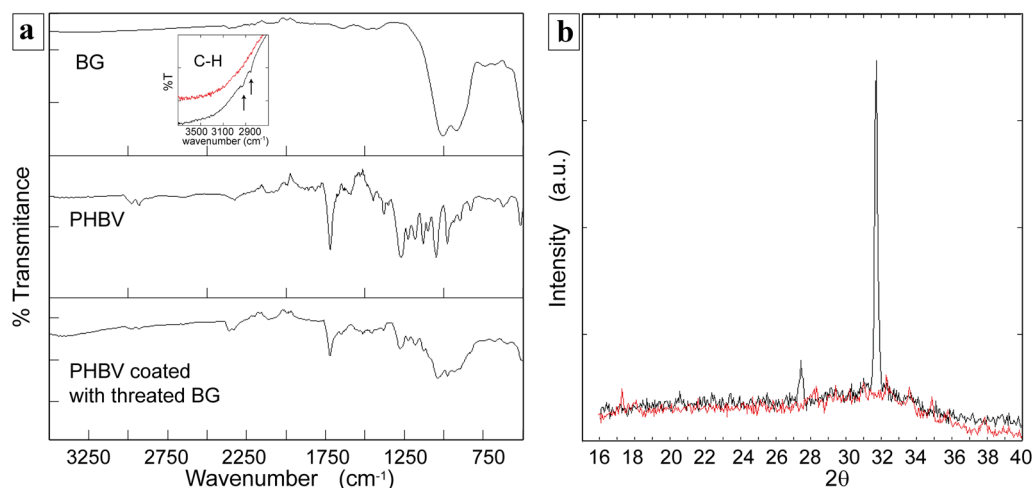


Figure 1: (a) IR-ATR spectra for CTMS-treated BG, PHBV scaffold, and PHBV coated with CTMS-treated BG scaffolds (from top to bottom). The inner panel in BG data shows DRIFT spectra of CTMS-treated (black line) and untreated (red line) BG. (b) WAXS data for CTMS-treated (black line) and untreated (red line) BG particles, showing crystal peaks corresponding to NaCl [21].

peaks in the diffractogram of the treated BG indicate a crystal-line structure. This corresponds to the periodic arrangement of NaCl [21, 22]. Because of the reaction of CTMS and silanol groups, Cl^- ions are released from CTMS in combination with Na ions that are present on the surface of BG particles. Since toluene was used as a solvent, the non-polar environment and solvent evaporation guided the formation of NaCl crystals of 1 to 3 μm in size (Supplementary Information, Fig.S2).

The ATR-FTIR spectra of PHBV and PHBV coated with CTMS-treated BG scaffolds were analyzed to identify functional groups (Fig. 1a, middle and lower panels). The IR spectrum of the PHBV scaffold revealed an intense band at 1720 cm^{-1} associated with the C=O bond stretching, that corresponds to the

characteristic ester carbonyl group of polyhydroxyalkanoates. The C–H stretching from methyl and ethyl groups was assigned to the bands located in the spectral region around 2900 cm^{-1} [23, 24]. The IR spectrum of the PHBV coated with CTMS-treated BG scaffold resembles the spectra of both PHBV and CTMS-treated BG combined. The characteristic bands of the individual components are present in the spectrum of the coated scaffold, which confirms the presence of BG on the PHBV scaffold.

Morphology and mechanical properties of filaments

PHBV and PHBV + BG filaments of $1.70 \pm 0.05\text{ mm}$ in diameter, as shown in Fig. 2a, were extruded in a twin-screw

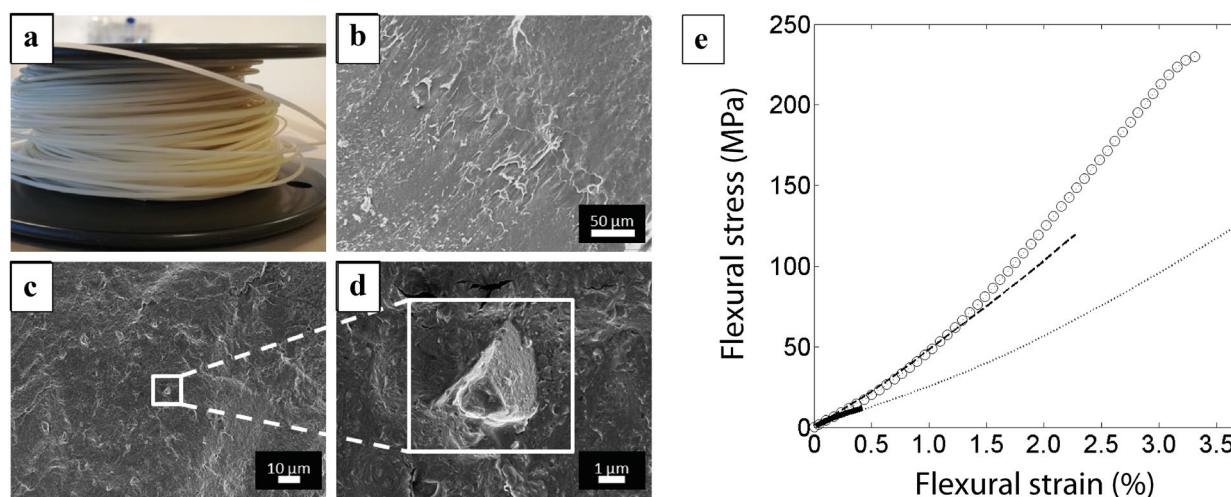


Figure 2: (a) Rolls of PHBV filaments obtained by powder extrusion (filaments diameter = $1.70 \pm 0.05\text{ mm}$). SEM image of the transversal section of the PHBV (b) and PHBV + BG (c) filaments (fracture surface). (d) Magnification of a CTMS-treated BG particle from image c. (e) Flexural stress–strain curves, measured in bending with a dual cantilever clamp, for filaments of PHBV (white dots), PHBV + BG (long dashed line), PHBV + untreated BG (solid line), and ABS (short dashed line).

mini-extruder. Figure 2b shows the transversal section of a PHBV filament; the material appears to be continuous and homogeneous without porosity at the observed scale. SEM analysis of a transversal section of PHBV + BG filaments shows BG particles homogeneously distributed in the polymer matrix (Fig. 2c and d).

Figure 2e presents the bending response of filaments made of PHBV, PHBV + BG, and PHBV + untreated BG. In order to compare to a well-known material used for 3D printing, the bending response of Acrylonitrile Butadiene Styrene (ABS) is also illustrated. Bending moduli, flexural strength, and the elongation at break of the tested samples are presented in Table 1. Extruded filaments composed of PHBV and untreated BG were too fragile to be manipulated, the flexural strength was lower than 10 MPa and elongation at break was 0.4% (Supplementary Information, Fig. S1). However, when BG treated with CTMS was extruded with the PHBV powder remarkable changes in the mechanical behavior of the filaments were observed. The flexural strength and the elongation at break increase up to 120 MPa and 2.3%, respectively. Compared to PHBV and ABS, PHBV + BG is more rigid.

Morphology and mechanical properties of scaffolds

Well-defined 3D printed structures of PHBV and PHBV + BG scaffolds are shown in Fig. 3. Strands are well adhered from one layer to the consecutive one. Figure 3a and b show 3-layer scaffolds printed with different $I_{\%}$. The printed structure has a smooth surface, open pores, and long interconnected vertical channels, illustrated in Fig. 3c. Vertical channels pass through the layers of the scaffold and have a transversal area that can

be tuned by the $I_{\%}$, from 4.76 to 0.04 mm², when $I_{\%}$ changes from 20 to 75%, Table 2. Furthermore, vertical channels are connected through the open pores, delimited by consecutive printed lines in the printing plane (xy) and two layers in the perpendicular direction (z). Regarding open pores, their volume is determined by their transversal area and the raster width ($480 \pm 30 \mu\text{m}$ according to the inner diameter of the nozzle). The transversal area depends on the layer height and the air gap between rasters (determined by $I_{\%}$) as represented in the lower panel of Fig. 3e; this area varies from 0.82 to 0.07 mm² when the $I_{\%}$ changes from 20 to 70%.

Figure 3d shows SEM images of PHBV scaffolds coated with CTMS-treated BG. The coating process leads to a fairly homogeneous covered surface of the scaffold. The upper panel in Fig. 3e evidences the suitable anchoring of BG particles to the surface of the scaffold.

The elastic behavior of the PHBV (black dots) and PHBV + BG (white dots) scaffolds was determined from tensile tests at 24 °C. It is important to remark that the elastic behavior of scaffolds was evaluated considering the transversal area of the scaffolds calculated as the nominal area to highlight the effect of the $I_{\%}$ on it. If just the area of the printed lines is considered to calculate the tensile stress, the elastic modulus remains constant (Supplementary Information, Fig. S3). Figure 3f shows the dependence of the tensile modulus (E) as a function of $I_{\%}$; E varies linearly from 250 ± 50 MPa to 1370 ± 108 MPa when $I_{\%}$ ranges from 20 to 90%. The linear tendency (dashed line in Fig. 3f, $R^2 = 0.9832$) is given by $E = E_0(0.011 I_{\%} - 0.096)$, where $E_0 = 1600$ MPa is the tensile modulus of PHBV. Regarding the effect of the BG coating on

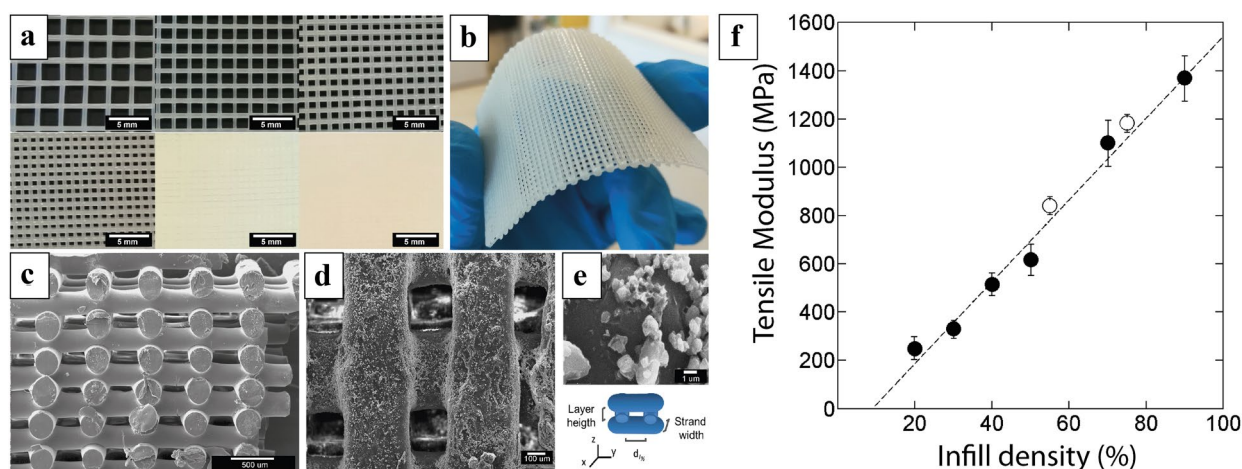


Figure 3: (a) PHBV scaffolds printed with 3 layers and 20, 30, 40, 50, 70, and 90% of $I_{\%}$ from top left panel to bottom right panel. (b) Example of the PHBV + BG printing quality and flexibility ($I_{\%} = 55\%$, 3 layers, nozzle inner diameter = 500 μm). (c) SEM image of the transversal section of a 3D printed PHBV scaffold ($I_{\%} = 50\%$, 12 layers, nozzle inner diameter = 300 μm). (d) Surface of PHBV scaffold coated with BG particles ($I_{\%} = 55\%$, nozzle inner diameter = 300 μm). (e) Magnified SEM image of the BG particles anchored to the polymer surface (upper panel) and scheme of the printing parameters that affect the area and volume of the open pores (lower panel) where $d_{\%}$ represents the air gap between rasters. (f) Linear correlation between the tensile modulus of PHBV (black dots) and PHBV + BG (white dots) scaffolds and the infill density ($I_{\%}$).

the elastic behavior of a scaffold, for instance, with 50% $I_{\%}$, E of a PHBV scaffold coated with BG was 590 MPa, similar to the value obtained for the PHBV scaffold (617 MPa). These results suggest that both, as a constituent of the filament and as a coating, BG did not affect the mechanical behavior of the polymer matrix at a concentration of 4 wt%.

Scaffolds bioactivity in simulated body fluid

In order to study the *in vitro* bioactivity, scaffolds were soaked for fixed periods in SBF at 36.5 °C. Figure 4 shows SEM images of the sample surfaces after 4 weeks of immersion. The image in Fig. 4a confirms the formation of structures with cauliflower shape compatible with a CHA-like formation [9]. The Ca/P proportion obtained by EDS is approximately 1.58. The Ca/P ratio in pure crystalline HA is 1.66, thus the lower value determined in the present case indicates that under the experimental conditions, the formed HA is carbonated (similar to natural bone)

and thus has low crystallinity [25]. Moreover, the cauliflower structures formed inside the superficial scratches (Fig. 4b) suggest that the SBF interacts with the BG leading to the formation of HA by heterogeneous nucleation. There was no HA formation in the PHBV scaffold observed under the microscope (data not shown). Furthermore, during the immersion period in SBF, at physiological temperature, there was no debonding between the printed layers, indicating the structural integrity of the fabricated scaffolds.

Cell response to materials and surface treatment

PHBV scaffolds

The *in vitro* behavior of NIH/3T3 cells on PHBV scaffolds was evaluated according to the international standard ISO10993-5, applicable to biomedical devices. Figure 5a shows a monolayer of normal fibroblasts grown in presence of the culture medium

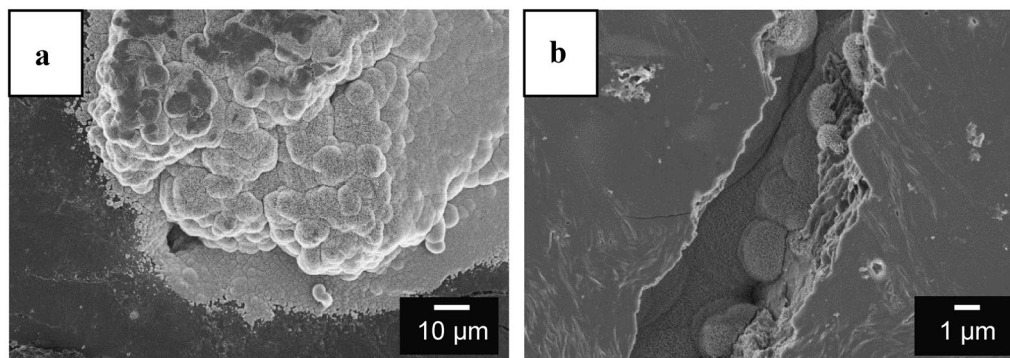


Figure 4: SEM images of HA structures formed on PHBV + BG scaffolds after 4 weeks of immersion in SBF. (a) HA cauliflower-shaped on the scaffold's surface. (b) Heterogeneous nucleation of HA onto the inner walls of a scratch.

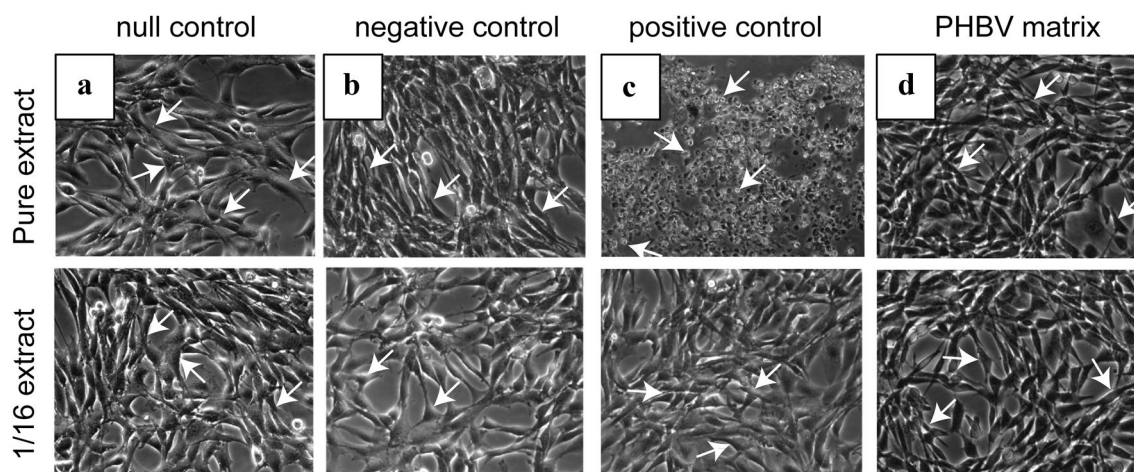


Figure 5: Morphological studies of NIH/3T3 on PHBV scaffolds evaluated by contrast phase microscopy—total magnification $\times 100$. Microscopy images of cell cultures used in the indirect assay where two extract dilutions were tested, pure extract (top panels) and 1/16 dilution (bottom panels). Four groups were studied: (a) null control (culture medium), (b) negative control (Teflon[®]), (c) positive control (Latex[®]) and (d) the PHBV scaffold. The arrows spot cells.

pure extract (null control) and in a 1/16 dilution. Cells presented a normal flattened spindle shape. Figure 5b shows fusiform cells due to the effect of the extract obtained from the medium with the negative control, Teflon®, at both tested dilutions. When cells were exposed to pure or diluted extracts of the medium with the positive control (Latex®), they became round-shaped without cytoplasmic extensions, being a sign of a cytotoxic effect in the pure extract. In the 1/16 dilution image, cells are fusiform and no cytotoxic effect was observed, Fig. 5c. Finally, Fig. 5d shows cells subjected to medium with extracts using the PHBV printed scaffold; these cells display a shape similar to the negative and null control groups. The indirect assay for the printed scaffold indicated grade 1 cytotoxicity, that is, low reactivity. From the cytotoxicity point of view, this result is promising to consider the PHBV scaffolds obtained by FDM for biomedical applications.

PHBV + BG scaffolds

The viability of MC3T3-E1 cells was evaluated through the indirect cytotoxicity assay to assess the biocompatibility of PHBV and PHBV + BG scaffolds through a colorimetric assay (WST-8 assay). The results presented in Fig. 6a demonstrated that the cell viability of both scaffolds increased compared to the control. The toxic influence of different DMSO concentrations shows the sensitivity of the test. Thus, PHBV and PHBV + BG scaffolds exhibit non-toxic effects on MC3T3-E1 cells.

Figure 6b shows the amount of adhered MC3T3-E1 cells on PHBV and PHBV + BG scaffolds. Cells adhered well to the scaffold struts, spread to attain proper cellular morphology, and remained viable since there is a correlation between Calcein AM and DAPI staining (green channel, Calcein and blue channel, DAPI, in Fig. 6b). These results suggest that PHBV and PHBV + BG scaffolds and their short-term degradation products

were non-toxic and suitable for cell culture. Moreover, the quantity of cells on the surface of PHBV + BG scaffolds is larger than that on PHBV scaffolds.

PHBV coated with CTMS-treated BG scaffolds

Stem cell attachment to the scaffolds made of PHBV and coated with CTMS-treated BG was evaluated at two different levels: cell population and single cell.

At a cell population level, cell behavior on the scaffolds was quantitatively evaluated by considering the MC3T3-E1 attachment to the surface. Cells cultured on the PHBV scaffolds adhered and this adhesion increased proportionally to the initial number of cells seeded (Fig. 7a, grey bars). Interestingly, there is a significant increase in adhered cells when comparing BG-coated scaffolds with uncoated scaffolds (Fig. 7a, black bars compared with grey bars). To assess cell viability, cells attached to the scaffolds were subsequently tripinized and re-cultured in the culture plates. Figure 7b showcases that cells previously attached to the PHBV scaffolds are able to proliferate and properly adhere to the multi-well plates. Accordingly, a higher cell density was observed in the wells from cultures in which 2×10^5 cells were initially seeded.

At a single cell level, cell behavior on the scaffolds was qualitatively evaluated by considering the morphology of rMSC attached to the scaffolds surface. Figure 7c and d show representative SEM images of cells adhered on scaffold surfaces. Typically, stem cell phenotypic expression of the rMSC was observed. The attached cells exhibited an extended morphology with thick structures; cell edges have thin and long prolongations that tend to embrace the BG particles (white arrows in the figure). It seems that cells try to maximize contact with the BG particles by means of these prolongations. It is apparent that

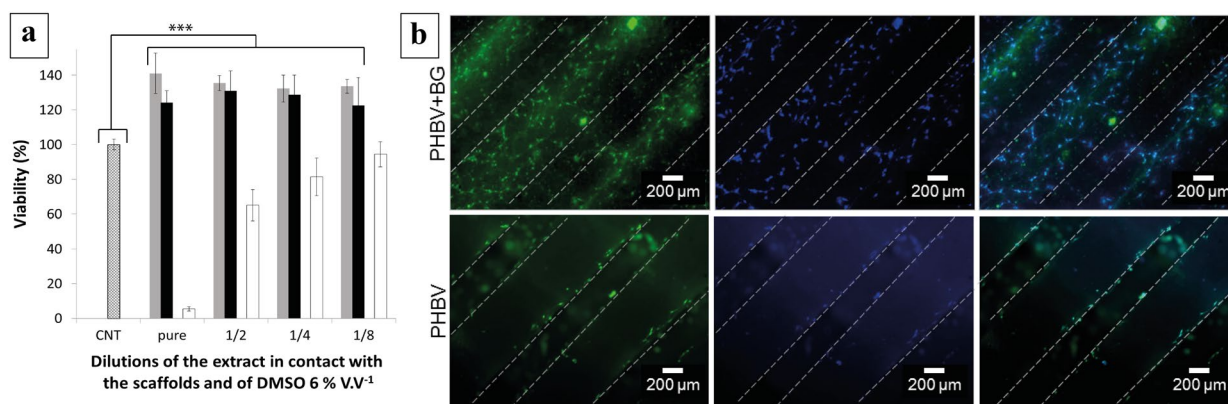


Figure 6: (a) Indirect in vitro biocompatibility test results: cell viability of MC3T3-E1 cells after 24 h of incubation with the extract of the supernatant from the scaffolds collected after 24 h. Grey bars correspond to PHBV + BG scaffolds and black bars to PHBV scaffolds, both at different supernatant concentrations. CNT corresponds to the control. Results are presented as a percentage of positive control (100%), with bars corresponding to 6% $V.V^{-1}$ DMSO which was used for the toxic reference. Significant differences between extracts in contact with scaffolds and CNT were found ($p \leq 0.001$, ***). (b) Fluorescence microscopy images of Calcein AM/DAPI staining of MC3T3-E1 adhered on PHBV and PHBV + BG scaffolds. Left panels show the Calcein fluorescence (green channel), middle panels show DAPI fluorescence (blue channel) and right panels show the merge of both channels.

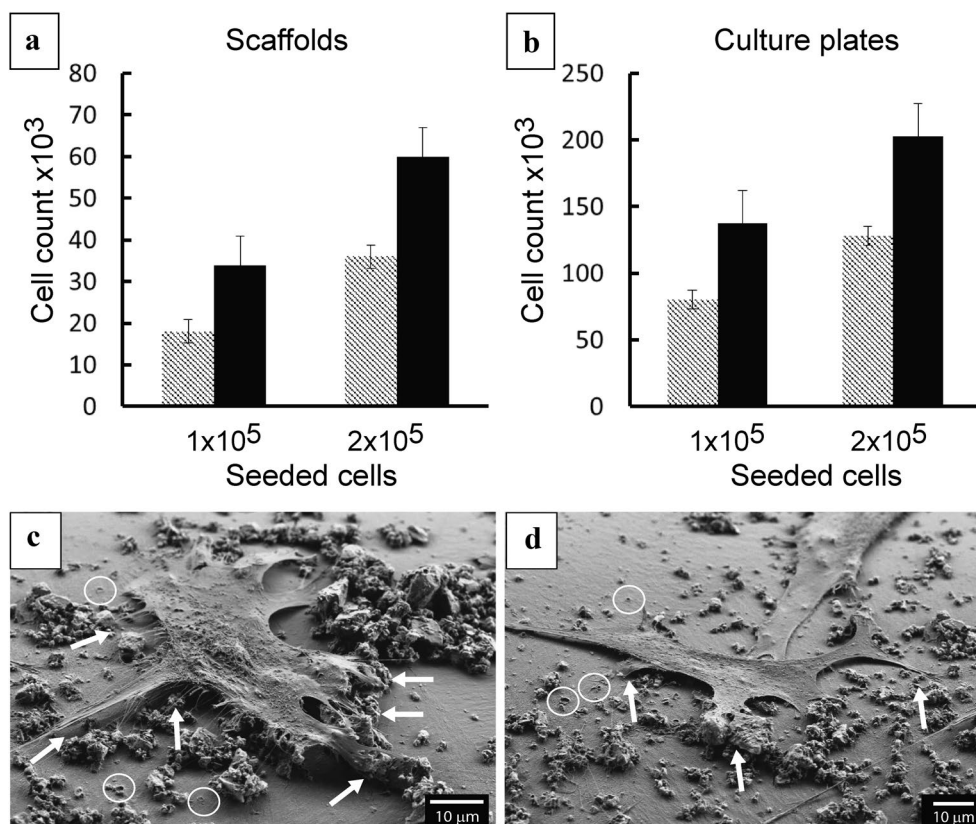


Figure 7: (a) and (b) Increased attachment of MC3T3-E1 cells onto PHBV coated with CTMS-treated BG scaffolds (black bars) compared to PHBV scaffolds (grey bars). (a) Cell counting attached to the scaffolds and (b) cell counting in culture plates after being attached to the scaffolds. Significant differences between scaffolds ($p < 0.05$). SEM images of rMSC adhered on the scaffold surface (c, d). The arrows spot cell anchoring points and the circles mark particles detached from the polymer surface.

TABLE 1: Mechanical properties of PHBV, PHBV+BG, and ABS tested in bending.

Material	Bending modulus (GPa)	Flexural strength (MPa)	Elongation at break (%)
PHBV	3.5 ± 0.3	230 ± 20	3.3%
PHBV+BG	4.6 ± 0.2	120 ± 18	2.3%
ABS	2.4 ± 0.1	Not measured*	Not measured*

*ABS did not break at testing.

cells prefer to attach to BG particles more than to the polymer surface, which is in agreement with early work on PDLA/BG composites [26]. The circles in both images mark part of the particles detached from the surface, leaving pores on the surface. This detachment of particles was not observed in SEM images

TABLE 2: Morphological characteristics of scaffolds controlled by the $l_{\%}$.

$l_{\%}$	20%	30%	40%	50%	70%	75%
Vertical channel size (μm) $\pm 5\%$	2182	1394	824	588	240	190
Vertical channel transversal area (mm^2) $\pm 10\%$	4.76	1.94	0.68	0.35	0.06	0.04
Horizontal channel transversal area (mm^2) $\pm 15\%$	0.82	0.51	0.27	0.17	0.07	0.05

(Fig. 3d) even though the scaffold was rinsed several times vigorously with distilled water.

Discussion

In this work, we present 3D printed composite scaffolds made from combination of PHBV and BG with tunable elastic and biological properties, suitable for bone regeneration. Although other scientists have successfully printed PHBV combined with fillers through various 3D printing techniques [15, 27–29], to the authors' knowledge, no work has been reported based on scaffolds made of PHBV combined with BG and printed by FDM to produce scaffolds for bone tissue engineering. The direct combination of PHBV and pristine BG particles results in filaments that are too brittle to be used in a commercial 3D

printer. This is probably due to the poor interaction between the hydrophilic surface of the BG particle and the hydrophobic polymer. This obstacle can be overcome and FDM can be used to prepare PHBV + BG filaments through a BG treatment with CTMS that yields a filament flexible enough to feed the printer. Particularly, the BG particle treatment was shown to lead to PHBV + BG filaments with flexural strain 5 times larger than that of PHBV filled with untreated BG. Although better mechanical properties are achieved, the decoration of the BG particle with a layer of $-\text{Si}-(\text{CH}_3)_3$ is too low to be considered the reason for this enhancement [30]. According to our preliminary results, it can be assumed that this enhancement might be due to NaCl micro-crystals formed along with the CTMS reaction on the surface of the BG particles in the organic solvent, as shown by WAXS (Fig. 1b). Annen et al. reported a similar process using a liquid chlorine donor in organic solvents to produce NaCl micro-crystals [22]. In fact, in the supplementary information (Supplementary Information, Fig. S1), a comparison of the flexural behavior of filaments made of PHBV + non-treated BG, PHBV + BG, and PHBV + NaCl particles showed that the presence of NaCl enhances the ductility. The influence of the NaCl micro-crystals (Supplementary Information, Fig. S2) due to the BG treatment is much lower probably because of its reduced size and concentration. Nevertheless, further work is required in order to establish the effect of NaCl particles on the spherulite size and mechanical properties of the polymeric phase.

Regarding the printing process, the printing temperature of PHBV and PHBV + BG filaments produced in this work can be accessed through the majority of the widespread FDM 3D printers, leading to an easy-to-use material for experimental printers. Moreover, the printed scaffolds present excellent reproducibility, printing fidelity, and proper layer adhesion. The mechanical and immersion tests indicated that the scaffolds showed enough structural stability for supporting safe handling. The 3D printing technique allows obtaining porous structures with pore sizes that can be mainly controlled by the printer parameter: the infill density. The infill density defines the distance between rasters, leading to a porous structure. Thus, the infill density clearly affects the scaffold porosity: decreasing the porosity of the scaffold by increasing the infill density. Consequently, printed scaffolds have channels that are fully interconnected through open pores. These channels are necessary to guide cell migration and cell ingrowth enabling the supply of nutrients, metabolites, and the elimination of waste products. In addition, internal vertices in the channels can be used as anchoring points for cells [31]. Cells attach first to the edge of pores and then they grow into the scaffolds through the interconnected pores [32, 33]. According to previous reports, the best pore size for short term cell growth is between 90 and 150 μm since it facilitates bone cell attachment; however, optimal cell proliferation, infiltration, and vascularization were found in scaffolds with pore

sizes in the range of 300–800 μm [34–37]. Nevertheless, these results depend mainly on cell type, material composition, and fabrication method. Both channel and pore sizes on the scale of 100–800 μm , as proposed in the literature, are achievable by the combination of the PHBV, BG, and FDM (Fig. 3). The effect of porosity on mechanical properties, in addition to the morphology, is an important factor when trying to mimic the complex structure–functionality relationship of natural bone [38]. Our results show that the air gap between rasters, tuned by the I_{90} , also defines the tensile modulus (Fig. 3f). Tensile modulus of scaffolds increased with the I_{90} , being the scaffold printed with 90% infill the one with the highest tensile modulus, close to the elastic modulus of the PHBV filament. Similar results were reported by Fernandez-Vicente et al. [39] for 3D printed ABS and by Akhoundi et al. [40] and Abeykoon et al. [41] for PLA. Interestingly, the addition of BG does not modify the tensile modulus of PHBV scaffolds, probably due to the low BG content. Thus, the morphology and the mechanical properties of scaffolds can be tailored by the printing conditions according to the specific bone tissue to regenerate.

MC3T3-E1 cells and rMSC were considered to assess the in vitro response to the scaffolds. PHBV + BG and PHBV scaffolds dissolution products were found to be not cytotoxic to MC3T3-E1 cells, and cells adhered more to the PHBV + BG surface than to the PHBV surface. Although PHBV scaffolds do not have osteoconductive properties nor a rough surface in the micrometric scale as anchoring points, MC3T3-E1 cells could adhere to the PHBV scaffold, in accordance to the work of Kumarasuriyar et al., who demonstrated PHBV ability to support osteoblast cell function [42].

In PHBV + BG scaffolds, cell contact to the BG particles depended on the rate of degradation of the polymer scaffold. In the case of PHBV, this process can take several months to expose the surface of a treated BG particle to the cells. An interesting design strategy to assess the interaction of cells with the CTMS-treated BG particles in a polymeric environment is to coat the scaffolds with CTMS-treated BG. The coating of polymeric scaffolds with BG particles has been explored before in order to increase the bioactivity of hydrophobic polyesters [43]. This process also increases the surface roughness of scaffolds, as well as being useful to assess the cytotoxicity of the CTMS treatment and the coating process. In an effort to anchor to the surface, rMSCs cells were seen to produce prolongations to attach themselves mainly to the BG particles and less to the PHBV surface (Fig. 7c and d). This coating process allows cells to attach more to the rough surface, in accordance with a previous report by Detsch et al., who showed that rMSC cells cultured on structured BG surfaces preferred a minimal surface roughness [44]. Compared to the PHBV scaffolds, those coated with CTMS-treated BG particles exhibited a higher number of MC3T3 cells adhered to the surface. These results demonstrate on one hand,

that the CTMS treatment is non-toxic and, on the other hand, that the strategy of coating scaffolds with BG improves cell adhesion by increasing cell anchorage sites. During immersion in culture medium, very few particles detached; this occurred perhaps spontaneously or particles were taken off by cells that were trying to anchor to the surface (Fig. 7c and d) or as a result of the dissolution of the NaCl micro-crystals anchored to the polymer surface. Even though the NaCl formation was not quantified, it is worth mentioning that on scaffolds coated with CTMS-treated BG, the NaCl crystals dissolve easily in the culture medium because of the high solubility of NaCl and may not be sensed by the cells. However, in the case of PHBV + BG scaffolds, NaCl micro-crystals are inside the polymeric matrix.

The bioactivity of a material in relation to bone tissue is usually evaluated by studying the ability to form a carbonated HA layer (HCA) on its surface upon immersion in SBF [45]. HCA is quite similar to the mineral phase that composes the bones. The presence of HCA on the surface of the material promotes the adhesion of biomolecules, cells, and growth factors involved in the creation of new bone and induces the binding to preexisting bone tissue. The immersion of PHBV + BG scaffolds in SBF demonstrated their ability to promote the formation of an HCA layer in a static environment, both on the scaffold surface and in scratches, despite the CTMS treatment of BG. It is worth mentioning that Chen et al. also reported that the chemical modification of BG with silanes does not compromise its bioactivity [46]. Many scientific works have been carried out regarding the surface modification of bioactive glasses in order to improve bioactivity, binding of biomolecules, attachment, proliferation, and differentiation of cells, as well as for drug delivery and antimicrobial applications, among others [47].

This work presents a process that allows fabricating a biodegradable and biocompatible filament of PHBV combined with BG particles with optimal mechanical properties for FDM, without adding commercial plasticizers. The morphological characteristics, mechanical properties, and biocompatibility of 3D printed PHBV + BG, PHBV and PHBV coated with BG are promising so that the scaffolds have great potential for bone tissue engineering applications.

Conclusions

In this work, 3D printed scaffolds capable of mimicking the bone extracellular matrix are presented. A filament based on PHBV loaded with BG particles exhibiting excellent flexibility was achieved by incorporating NaCl crystals and slightly modifying the BG surface with CTMS. Furthermore, it was shown that this treatment does not compromise the BG bioactivity. The BG and PHBV combination leads to a bioactive and bioresorbable composite scaffold with mechanical properties that can be tailored by changing one of the main printing parameters: the

infill density. Moreover, the strategy of coating scaffolds with BG particles incorporates micrometer features to the smooth scaffold surface increasing cell adhesion. In future, PHBV + BG scaffolds coated with BG should be further characterized, e.g. in vivo, for assessing their suitability for bone tissue engineering.

Materials and methods

Materials

Polyhydroxybutyrate-co-hydroxyvalerate (PHBV) in powder form from Tianan (China), brand name ENMAT Y1000, containing 1.5 mol% valerate without additives was used as received. 45S5 BG powder (5 μm mean particle size) was used (Schott AG, Germany). Chlorotrimethylsilane (CTMS) from Sigma-Aldrich was used as a silylating agent on the BG surface treatment. Toluene and chloroform analytical grade were used as solvents.

Bioglass particle treatment

The surface of the BG particles was treated by immersion in a solution of 10% v.v⁻¹ CTMS in toluene, evaporated at room temperature, and dried under vacuum in a desiccator overnight [48]. Reaction products were studied by Wide-angle X-ray scattering Xeuss 2.0 SAXS/WAXS instrument from Xenocs. Diffuse Reflectance Infrared Fourier Transform (DRIFT) measurements were collected using a Thermo Nicolet iS50 Advanced spectrometer (Thermo Fisher Scientific Co., Waltham, MA, USA) to evaluate the BG silylation reaction. (In what follows BG is used to refer to BG treated with CMTS).

Filament fabrication

PHBV and PHBV + BG filaments were produced by extrusion in a twin-screw mini-extruder (Thermo Fisher Scientific Process 11). PHBV + BG filament contains 4 wt% of BG. Prior to extrusion, PHBV and BG (untreated and treated with CTMS) powders were dried in a vacuum oven over night at room temperature. Temperature profile and extrusion speed were carefully set to minimize the thermal degradation of the materials.

Scaffolds fabrication

Scaffolds were fabricated by FDM in a 3D printer Codex 2020, using a rectilinear infill pattern. Scaffolds were designed in SolidWorks® and then converted to a file readable by the 3D printer. The printer barrel was covered by polytetrafluoroethylene (PTFE) and a nozzle made of stainless steel of 500 μm inner diameter was used. The optimization process of FDM was carried out by adapting the typical parameters for 3D printing using ABS and PLA (not reported here). The printing temperature was adjusted to 196 °C based on the processing temperature

during filament extrusion (maximum temperature profile ~ 190 °C) [49]. Thus, the temperature was set low enough to avoid overheating of the material and sufficiently high to get good adhesion between layers and to the bed. The printing speed was adjusted at 11 mm·min⁻¹ to avoid hot spots on the scaffolds, allowing uniform cooling of the printed lines before starting to print the consecutive layers and preventing regions of overheating where the structure would collapse, without compromising the layer adhesion. The bed temperature was maintained at 100 °C to minimize thermal shrinkage and to avoid warping. The printing process was performed in a printing chamber to assure thermal stability during the scaffold fabrication. The layer height was 300 μm, set as 60% of the nozzle diameter, leading to adequate layer adhesion. All these parameters were kept constant for all the experiments because they affect the mechanical properties and morphology of scaffolds [50, 51]. Thus, the infill density (measured in percent, $I_{\%}$) was varied in order to study its effect on the mechanical properties of scaffolds made of PHBV or PHBV + BG filaments.

Some of the PHBV scaffolds were coated with BG in order to assess possible differences in the behavior of the seeded cells with respect to non-coated PHBV scaffolds. Briefly, the PHBV scaffold was sonicated in chloroform for 8 min to slightly dissolve the polymer surface; due to this process, the surface of the scaffold becomes soft and sticky. Then, the scaffold was immersed in a suspension of (CTMS-treated) BG in chloroform, sonicated for 2 min, and dried at 170 °C for less than 8 min. The heating process fixes the BG particles and eliminates the solvent. Then the scaffold was rinsed several times with distilled water to remove any loose particle of BG. Finally, any residual solvent was eliminated by drying the scaffold overnight in a vacuum oven at room temperature.

Morphological and chemical characterization

The structure of filaments and scaffolds was explored by scanning electron microscopy (Carl Zeiss NTS SUPRA 40 from the Advanced Microscopy Center (CMA) and Philips XL30 Serie 30). Samples were cryogenically cut in liquid nitrogen and coated with a thin layer of Au–Pd (40:60). The chemical composition was evaluated by FTIR-ATR by direct analysis of the samples on ZnSe crystal. Infrared spectra were obtained on an FTIR Nicolet 8700 (Thermo Scientific) spectrophotometer with 32 scans, a resolution of 4 cm⁻¹, and an interval of 2 cm⁻¹.

Mechanical characterization

Bending of the filaments and tensile properties of the 3D printed scaffolds were tested in a DMA Q800 (TA Instruments). Particularly, the bending test resembles the flexure of the filament during FDM, e.g. exerted by the tube that guides it from the feeder

to the hot end of the printer. Elastic or flexural moduli were obtained from the slope of the tensile or bending stress–strain curve, respectively. Tensile and flexural tests were made at 10 μm min⁻¹ and 2% min⁻¹, respectively. Sample dimensions of 3D printed scaffolds were 6.0 mm × 1.0 mm × 20.0 mm and the tensile test was performed in the same direction for all the samples. The transversal area was calculated as the nominal area to highlight the effect of $I_{\%}$ on the tensile modulus. All experiments were performed in sextuplicate.

Bioactivity in simulated body fluid

In vitro bioactivity was studied in simulated body fluid (SBF) according to Kokubo et al. [52]. Specimens consisting of one printed layer and 100% $I_{\%}$ (10.0 mm × 10.0 mm × 0.5 mm) were soaked SBF at 36.5 °C for different periods within 30 days. The SBF solution was changed every 3 days. The HA-like layer formation was characterized by SEM–EDS [53] (from CMA). The experiment was performed by triplicate.

In vitro analysis

In order to examine the interactions of our materials in the best possible way in terms of cell biology, firstly fibroblastic cells (NIH/3T3) were used for initial cytocompatibility studies, followed by the application of osteoblasts (MC3T3-E1) for detailed and direct contact investigations. Finally, primary stem cells (rMSC) were utilized for high magnification morphological analyzes.

Cytotoxicity of PHBV scaffolds

Indirect contact assay was performed, according to ISO10993-5, to assess the in vitro cytotoxicity of the scaffolds. The concept of the indirect contact assay is to investigate the influence of release and degradation products of medical devices. PHBV samples printed with 50% $I_{\%}$ were rinsed several times with distilled water and sterilized in an autoclave. Complete medium (DMEM with 5% FBS), latex® rubber, and poly-tetrafluoroethylene (Teflon®, DuPont, DE) were considered as the null, positive and negative controls, respectively. Samples were incubated in complete medium with a material area (cm²): media (ml) ratio of 6:1 for 72 h at 37 °C in a humidified atmosphere containing 5% CO₂. 1 × 10⁵ mouse fibroblastic cells (NIH/3T3 cell line) were incubated in a 24-well plate (Corning Costar, MA) at 37 °C in a 5% CO₂ humidified incubator for 24 h. The culture medium of the cells was replaced by the medium that was incubated with the samples at two different concentrations: the pure extract and 1/16 dilution of the extract in complete medium. Cells were incubated within the extracts for 24 h. The cytotoxicity of PHBV was assessed qualitatively: cells were examined microscopically in a Nikon TE2000-U inverted microscope coupled

to an ORCA-ER CCD camera (Hamamatsu), at a total magnification of $\times 100$. Changes in general morphology, vacuolization, detachment and cell lysis were assessed. All experiments were performed in triplicate.

MC3T3-E1 on PHBV and PHBV + BG scaffolds

The MC3T3-E1 (Sigma-Aldrich, Germany) cells, immortalized pre-osteoblastic cells derived from C57BL/6 mouse calvaria, were cultured at 37 °C in an atmosphere of 95% humidified air and 5% CO₂, in a solution of MEM alpha (Dulbecco, Germany) containing 10 vol% of fetal bovine serum (FBS, Sigma-Aldrich, Germany), 1 vol% of penicillin/streptomycin (Life technology, Germany) and 1 vol% of L-Glutamine (Life technology, Germany). *WST-8 assay*: Scaffolds (0.1 g ml⁻¹) were soaked in this cell culture medium at 37 °C with 5% CO₂ for 24 h after sterilizing both surfaces using UV light for 30 min. Afterwards, cells (P14) were seeded into 24-well plates (100,000 cells ml⁻¹) and also cultured in a cell culture medium for 24 h at 37 °C with 5% CO₂. Then, the cell culture medium of cells was replaced by different dilutions of the extract of the supernatant from the scaffolds collected after 24 h (pure, 1/2, 1/3, 1/4) and fresh cell culture medium as a positive as well as 6 v.v⁻¹% DMSO (dimethyl sulfoxide; pure, 1/2, 1/3, 1/4) as negative references at 37 °C with 5% CO₂ for 24 h. Afterwards, the WST-8 assay (5%, supplied by Sigma Aldrich) was used to determine the influence of the released compounds/ions on the viability of treated cells using a PHOmo microplate reader (Autobio Diagnostics Co., China) to measure the dye absorbance, *Abs*. The cell viability percentage was calculated considering the positive control as 100% using the following equation:

$$\text{Viability\%} = \frac{\text{Abs}_{\text{treated cells}} - \text{Abs}_{\text{blanc}}}{\text{Abs}_{\text{cell control}} - \text{Abs}_{\text{blanc}}} \times 100\%$$

Calcein AM/DAPI assay scaffolds (75% infill) were UV sterilized for 30 min (for each side) and pretreated in cell culture medium for 7 days. After this period, cells (100,000 cells ml⁻¹) were seeded on the scaffolds and incubated for 24 h. All living cells were stained with Calcein AM/DAPI (supplied from Thermo Fisher) and cell adhesion was evaluated via fluorescence microscopy images (Zeiss, Germany) using the software ImageJ.

MC3T3-E1 on PHBV coated with CTMS-treated BG scaffolds

A procedure was conducted with MC3T3-E1. Two PHBV scaffolds and two PHBV scaffolds coated with CTMS-treated BG were sterilized at 121 °C in an autoclave and were deposited in a 24-well plate. 1×10^5 and 2×10^5 cells were seeded onto each printed structure and in adjacent empty wells as a control group. After incubating for 24 h, the scaffolds were removed, washed twice with PBS, and incubated for 48 h with 1 ml medium. After this period, scaffolds were removed and washed twice with

PBS. Cells on the printed struts were detached with trypsin; an aliquot was separated and counted in a Neubauer chamber. Cells were incubated for 72 h and observed under a Leica DMi1 inverted microscope, with a Digital microscope camera Leica MC120 HD in order to determine the presence of adhered cells and the confluence in each well. Finally, cells were treated with trypsin and counted in Neubauer chamber.

rMSC on PHBV coated with CTMS-treated BG scaffolds

Adhesion of rat mesenchymal stem cells (rMSC), which are ideal tools for morphological studies on biomaterials [44], onto PHBV coated with treated BG scaffold was evaluated qualitatively. These rMSC were isolated from rat bone marrow as described by Schrepper et al. [54] (isolated, disrobed, and provided by the Department of Plastic and Hand Surgery, Universitätsklinikum Erlangen). Before cell seeding, samples were sterilized at 121 °C in an autoclave (Systec, Germany) and pre-incubated in culture medium for 48 h. rMSCs were inoculated (100,000 cells ml⁻¹, total 30,000 cells sample⁻¹) and cultured for 24 h; morphological phenotype analysis was performed by SEM [44].

Statistical methods

The results are presented as the mean S.D. ANOVA (analysis of variance) and a student's *t*-test were carried out to determine the significant differences among the groups. The observed differences were statistically significant when $p < 0.05$.

Acknowledgments

The authors would like to acknowledge PhD. Mariana Hamer for technical support on DRIFT (Nanosystems Institute, ECyT, UNSAM); PhD Cristián Huck for technical support on WAXS (Laboratory of Applied Crystallography, ECyT, UNSAM) and I. D. Adrian Oviedo for technical support on filament extrusion process (Nanotechnology Argentinian Foundation).

Author contributions

BA: Conceptualization, Methodology, Investigation, Writing—Original Draft, Writing—review and Editing, Project Administration. EK, AGW, RD, JB, GG: Methodology, Investigation. ARB: Funding Acquisition, Project Administration, Supervision, Discussion, Review, Resources. ÉBH: Funding Acquisition, Project Administration, Supervision, Discussion, Review, Resources.

Funding

This work was supported by the Program of Bilateral Cooperation Level 1 (PCB-11) with CONICET-BAYLAT (Bayerische Hochschulzentrum für Lateinamerika). Projects of Innovation,

Development, and Adoption of 3D Printing Technology, of the Ministry of Science, Technology and Productive Innovation (MINCyT). UNSAM and CONICET.

Data availability

The datasets generated during and/or analysed during the current study are available from the corresponding author on reasonable request.

Declarations

Conflict of interest On behalf of all authors, the corresponding author states that there is no conflict of interest.

Supplementary Information

The online version contains supplementary material available at <https://doi.org/10.1557/s43578-021-00272-9>.

References

- P. Tack, J. Victor, P. Gemmel, L. Annemans, *Biomed. Eng. Online* (2016). <https://doi.org/10.1186/s12938-016-0236-4>
- E.F. Morgan, G.U. Unnikrisnan, A.I. Hussein, *Annu. Rev. Biomed. Eng.* (2018). <https://doi.org/10.1146/annurev-bioeng-062117-121139>
- H. Li, R. Du, J. Chang, *J. Biomater. Appl.* (2005). <https://doi.org/10.1177/0885328205049472>
- J. Wu, K. Xue, H. Li, J. Sun, K. Liu, *PLoS ONE* (2013). <https://doi.org/10.1371/journal.pone.0071563>
- L.L. Hench, *J. Mater. Sci. Mater. Med.* (2006). <https://doi.org/10.1007/s10856-006-0432-z>
- J.R. Jones, *Acta Biomater.* (2013). <https://doi.org/10.1016/j.actbio.2012.08.023>
- L.L. Hench, *J. Eur. Ceram. Soc.* (2009). <https://doi.org/10.1016/j.jeurceramsoc.2008.08.002>
- H. Yuan, J.D. de Bruijn, X. Zhang, C.A. van Blitterswijk, K. de Groot, *J. Biomed. Mater. Res.* (2001). [https://doi.org/10.1002/1097-4636\(2001\)58:3%3c270::aid-jbm1016%3e3.0.co;2-2](https://doi.org/10.1002/1097-4636(2001)58:3%3c270::aid-jbm1016%3e3.0.co;2-2)
- K. Rezwani, Q.Z. Chen, J.J. Blaker, A.R. Boccaccini, *Biomaterials* (2006). <https://doi.org/10.1016/j.biomaterials.2006.01.039>
- E. Fukada, Y. Ando, *Int. J. Biol. Macromol.* (1986). [https://doi.org/10.1016/0141-8130\(86\)90056-5](https://doi.org/10.1016/0141-8130(86)90056-5)
- S. Gogolewski, M. Jovanovic, S.M. Perren, J.G. Dillon, M.K. Hughes, *J. Biomed. Mater. Res.* (1993). <https://doi.org/10.1002/jbm.820270904>
- I. Manavitehrani, A. Fathi, H. Badr, S. Daly, A. Negahi Shirazi, F. Dehghani, *Polymers (Basel)* (2016). <https://doi.org/10.3390/polym8010020>
- S. Bose, S. Vahabzadeh, A. Bandyopadhyay, *Mater. Today* (2013). <https://doi.org/10.1016/j.mattod.2013.11.017>
- S. Zhao, M. Zhu, J. Zhang, Y. Zhang, Z. Liu, Y. Zhu, C. Zhang, *J. Mater. Chem. B* (2014). <https://doi.org/10.1039/c4tb00838c>
- M.A. Vigil Fuentes, S. Thakur, F. Wu, M. Misra, S. Gregori, A.K. Mohanty, *Sci. Rep.* (2020). <https://doi.org/10.1038/s41598-020-68331-5>
- Á. Rivera-Briso, A. Serrano-Aroca, *Polymers* (2018). <https://doi.org/10.3390/polym10070732>
- B. Marelli, C.E. Ghezzi, J.E. Barralet, A.R. Boccaccini, S.N. Nazhat, *Biomacromol.* (2010). <https://doi.org/10.1021/bm1001087>
- Q. Fu, N. Zhou, W. Huang, D. Wang, L. Zhang, H. Li, *J. Mater. Sci. Mater. Med.* (2004). <https://doi.org/10.1007/s10856-004-5742-4>
- A. Tilocca, N.H. de Leeuw, *J. Phys. Chem. B* (2006). <https://doi.org/10.1021/jp065146k>
- L. Lefebvre, J. Chevalier, L. Gremillard, R. Zenati, G. Thollet, D. Bernache-Assolant, A. Govin, *Acta Mater.* (2007). <https://doi.org/10.1016/j.actamat.2007.01.029>
- C. Rodriguez-Navarro, L. Linares-Fernandez, E. Doehne, E. Sebastian, *J. Cryst. Growth* (2002). [https://doi.org/10.1016/S0022-0248\(02\)01499-9](https://doi.org/10.1016/S0022-0248(02)01499-9)
- T. Annen, M. Epple, *J. Chem. Soc. Dalton Trans.* (2009). <https://doi.org/10.1039/b911047j>
- Q. Liu, M. Zhu, W. Wu, Z. Qin, *Polym. Degrad. Stab.* (2017). <https://doi.org/10.1016/j.polymdegradstab.2008.10.016>
- A. Aramvash, Z. Akbari Shahabi, S. Dashti Aghjeh, M.D. Ghafari, *Int. J. Environ. Sci. Technol.* (2015). <https://doi.org/10.1007/s13762-015-0768-3>
- A.B.H. Yoruç, A. Aydınoglu, *Mater. Sci. Eng. C* (2017). <https://doi.org/10.1016/j.msec.2017.02.049>
- J.J. Blaker, V. Maquet, R. Jérôme, A.R. Boccaccini, S.N. Nazhat, *Acta Biomater.* (2005). <https://doi.org/10.1016/j.actbio.2005.07.003>
- B. Duan, W.L. Cheung, M. Wang, *Biofabrication* (2011). <https://doi.org/10.1088/1758-5082/3/1/015001>
- X. Ye, L. Li, Z. Lin, W. Yang, M. Duan, L. Chen, Y. Xia, Z. Chen, Y. Lu, Y. Zhang, *Carbohydr. Polym.* (2018). <https://doi.org/10.1016/j.carbpol.2018.08.117>
- P. Shuai, C. Guo, W. Gao, C. Yang, Y. Xu, Y. Liu, L. Qin, T. Sun, H. Yang, S. Feng, P. Wu, *Polymers* (2017). <https://doi.org/10.3390/polym9050175>
- N. Ren, L. Yang, T.Y. Zhao, Y.G. Zhao, *Key Eng. Mater.* (2008). <https://doi.org/10.4028/www.scientific.net/kem.368-372.1215>
- M. Rumpler, A. Woesz, J.W.C. Dunlop, J.T. van Dongen, P. Fratzl, *J. R. Soc. Interface* (2008). <https://doi.org/10.1098/rsif.2008.0064>
- I. Manjubala, A. Woesz, C. Pilz, M. Rumpler, N. Fratzl-Zelman, P. Roschger, J. Stampfl, P. Fratzl, *J. Mater. Sci. Mater. Med.* (2005). <https://doi.org/10.1007/s10856-005-4715-6>
- K.W. Lee, S. Wang, M. Dadsetan, M.J. Yaszemski, L. Lu, *Biomacromol.* (2010). <https://doi.org/10.1021/bm901260y>

34. Q.L. Loh, C. Choong, *Tissue Eng. B* (2013). <https://doi.org/10.1089/ten.TEB.2012.0437>
35. C.M. Murphy, F.J. O'Brien, *Cell. Adh. Migr.* (2010). <https://doi.org/10.4161/cam.4.3.11747>
36. S.H. Oh, T.H. Kim, G. Il Im, J.H. Lee, *Biomacromol* (2010). <https://doi.org/10.1021/bm100199m>
37. S.J. Lee, I.W. Lee, Y.M. Lee, H.B. Lee, G. Khang, *J. Biomater. Sci. Polym. Ed.* (2004). <https://doi.org/10.1163/1568562041526487>
38. V. Karageorgiou, D. Kaplan, *Biomaterials* (2005). <https://doi.org/10.1016/j.biomaterials.2005.02.002>
39. M. Fernandez-Vicente, W. Calle, S. Ferrandiz, A. Conejero, *3D Print Addit. Manuf.* (2016). <https://doi.org/10.1089/3dp.2015.0036>
40. B. Akhouni, A.H. Behraves, *Exp. Mech.* (2019). <https://doi.org/10.1007/s11340-018-00467-y>
41. C. Abeykoon, P. Sri-Amphorn, A. Fernando, *Int. J. Light Mater. Manuf.* (2020). <https://doi.org/10.1016/j.ijlmm.2020.03.003>
42. A. Kumarasuriyar, R.A. Jackson, L. Grøndahl, M. Trau, V. Nurcombe, S.M. Cool, *Tissue Eng.* (2005). <https://doi.org/10.1089/ten.2005.11.1281>
43. J. Roether, A. Boccaccini, L. Hench, V. Maquet, S. Gautier, R. Jérôme, *Biomaterials* (2002). [https://doi.org/10.1016/S0142-9612\(02\)00131-X](https://doi.org/10.1016/S0142-9612(02)00131-X)
44. R. Detsch, O. Guillon, L. Wondraczek, A.R. Boccaccini, *Adv. Eng. Mater.* (2012). <https://doi.org/10.1002/adem.201180068>
45. T. Kokubo, H. Takadama, in *Handbook of Biomineralization*, ed. by E. Bäuerlein (John Wiley & Sons, Ltd, 2007), p. 97–109
46. Q.Z. Chen, K. Rezwan, D. Armitage, S.N. Nazhat, A.R. Boccaccini, *J. Mater. Sci. Mater.* (2006). <https://doi.org/10.1007/s10856-006-0433-y>
47. V. Stanić, in *Clinical Applications of Biomaterials*, ed. by G. Kaur (Springer, New York, 2017), p. 35–63
48. B. Seed, *Curr. Protoc. Mol. Biol.* (1994). <https://doi.org/10.1002/0471142727.mba03bs28>
49. L.J. Vandi, C.M. Chan, A. Werker, D. Richardson, B. Laycock, S. Pratt, *Polym. Degrad. Stab.* (2019). <https://doi.org/10.1016/j.polymdegradstab.2018.10.015>
50. H.R. Vanaei, K. Raissi, M. Deligant, M. Shirinbayan, J. Fitoussi, S. Khelladi, A. Tcharkhtchi, *J. Mater. Sci.* (2020). <https://doi.org/10.1007/s10853-020-05057-9>
51. T.C. Yang, C.H. Yeh, *Polymers* (2020). <https://doi.org/10.3390/polym12061334>
52. T. Kokubo, H. Takadama, *Biomaterials* (2006). <https://doi.org/10.1016/j.biomaterials.2006.01.017>
53. M.J. Bailey, S. Coe, D.M. Grant, G.W. Grime, C. Jeynes, *X-Ray Spectrom.* (2009). <https://doi.org/10.1002/xrs.1171>
54. S. Schrepfer, T. Deuse, C. Lange, R. Katzenberg, H. Reichensperner, R.C. Robbins, M.P. Pelletier, *Stem Cells Dev.* (2007). <https://doi.org/10.1089/scd.2006.0041>